 doi:10.20944/preprints202011.0579.v1

Article

Few-Layered MoS_2 Nanoparticles Covering Anatase TiO_2 Nanosheets: Comparison between *ex-situ* and *in-situ* Synthesis Approaches

Rosangela Santalucia [1], Tiziano Vacca [1], Federico Cesano [1], Gianmario Martra [1], Francesco Pellegrino [1], and Domenica Scarano [1,*]

[1] Department of Chemistry, NIS (Nanostructured Interfaces and Surfaces) Interdepartmental Centre and INSTM Centro di Riferimento, University of Torino, Via P. Giuria, 7, 10125 Torino, Italy; rosangela.santalucia@unito.it, tiziano.vacca@edu.unito.it, federico.cesano@unito.it, francesco.pellegrino@unito.it, domenica.scarano@unito.it

* Correspondence: domenica.scarano@unito.it; Tel.: +39-011-6707834 (D.S.)

Devoted to Gianmario Martra

Abstract: MoS_2/TiO_2 nanostructures made of MoS_2 nanoparticles covering TiO_2 nanosheets have been synthesized, either via *ex-situ* or *in-situ* approaches. Morphology and structure of MoS_2/TiO_2 hybrid nanostructures have been investigated and imaged by means of X-ray diffraction (XRD) analysis and high-resolution transmission electron microscopy (HRTEM), while the vibrational and the optical properties have been investigated by Raman, Fourier-transform infrared spectroscopy (FTIR) and UV−visible (UV-Vis) techniques. The different stacking degrees together with the size distribution of the MoS_2 nanosheets, decorating the TiO_2 nanosheets, have been carefully obtained from HRTEM images. The nature of the surface sites on the main exposed faces of both materials has been detected by means of *in-situ* FTIR spectra of adsorbed CO probe molecule. The results coming from the *ex-situ* and *in-situ* approaches will be compared, by highlighting the role of the synthesis processes in affecting morphology and structure of MoS_2 nanosheets, including their curvature, surface defects, and stacking order. Some more, it will be shown that the *in-situ* approach is affecting the reactivity of the TiO_2 nanosheets too, hence in turn affects the MoS_2/TiO_2 nanosheets interaction.

Keywords: heterostructures; TiO_2 nanosheets; few layers MoS_2/TiO_2; *ex-situ* and *in-situ* approaches; FTIR; Raman; UV-Vis; XRD; HRTEM

1. Introduction

Heterostructures of different dimensionality have been exploited in the past few years because of their novel properties and challenging applications, including the developing of clean energy and new energy-related technologies, including photocatalysis [1,2], electrocatalysis [3], solar cells [4], energy conversion and storage [1,5] up to researches in the biomedical fields [6-8]. In particular, since the discovery of graphene, 2D materials have attracted considerable attention due to their unique physical and chemical properties. For this, many efforts have been focused on the combination of the two-dimensional layered materials (2DLMs) with the zero-dimensional ones (0D), such as plasmonic nanoparticles and quantum dots, with the mono-dimensional (1D) nanostructures, such as nanowires and nanoribbons, thus opening a new way for nanoscale material integration and enabling many extraordinary electronic devices. Along these themes, 2D−2D van der Waals heterostructures made of distinct 2DLMs and superlattices [8] play a considerable role in controlling and manipulating the generation, confinement and transport of charge carriers, excitons, photons and phonons within the atomic interfaces, thus giving chances for the design of unique and challenging devices [9-11].

Besides graphene-like and in general nanocarbon materials, prominent candidates for heterostructures and hybrid combinations belong to the family of semiconducting inorganic systems,

 doi:10.20944/preprints202011.0579.v1

such as nanostructured transition metal dichalcogenides (TMDs, i.e., MoS_2, WS_2) and oxides (i.e., TiO_2, perovskites) [12,13].

Notice that each layer within the two-dimensional layered materials (2DLMs) consists of a covalently bonded, dangling-bond-free lattice, which provides in-plane stability of 2D crystals, whereas relatively weak, van-der-Waals-like interactions are able to keep the neighbouring layers together [14,15]. This makes it feasible to isolate, mix and match highly different atomic layers to create a wide range of van der Waals heterostructures (vdWHs) without the constraints of lattice matching and processing compatibility, in a sequence with one-atom-plane precision [15-17].

Regard to this, a huge amount of MoS_2/TiO_2 based heterostructures with superior performance with respect to the individual MoS_2 and TiO_2-based materials has been obtained [18,19]. As a matter of fact, MoS_2 has been considered of great interest to perform MoS_2/TiO_2 hybrid composites, due to its absorption in the UV−visible range, and then its ability to increase the visible light absorption of TiO_2-based systems [20,21]. Conversely, TiO_2, despite being an excellent photocatalyst, it is known to absorb only a small portion of the solar spectrum in the UV region (3% of the sunlight spectrum) [22].

Therefore, in order to address the opportunities of new and advanced applications, a deeper understanding of the relationship between structure and properties in MoS_2/TiO_2-based composites has to be provided, Concerning this point, the lattice mismatch, that is, different lattice constants and atomic arrangements between MoS_2 and TiO_2 explains the tendency of TiO_2 particles to agglomerate, thus causing a poor interfacial contact of TiO_2 particles with the MoS_2 layered material. As it is known that the interface plays a key role in the charge carrier separation and migration [23], many efforts have been devoted to grow 2D MoS_2 nanosheets on stable 2D TiO_2 nanosheets as substrates, which provide a larger contact specific surface areas for charge carrier transfers [5]. In particular, 2D anatase TiO_2 nanosheets with exposed {001} facets [24] have attracted especially great interest in the nucleation and growth of the MoS_2 nanosheets [8,25].

Considering the favourable optical properties of MoS_2, that is, excitonic absorption bands in the visible and the efficient interfacial charge-transfer region [26] between MoS_2 nanoparticles and TiO_2 nanosheets, in recent years, highly dispersed MoS_2 nanostructures have been prepared via through different synthetic strategies, including *ex-situ* and *in-situ* approaches. It has been reported that, low cost and scalable production, highly heterogeneous MoS_2/TiO_2-based composites, but with weak interface interactions are obtained via *ex-situ* synthesis [5,19] whereas composites with strong interface contacts can be achieved, although at a low yield, from *in-situ* strategies [5]. It is known that the method allows the atomic scale assembling and then the growth of well-defined MoS_2 slabs, thus, ensuring a good chemical interaction at the interface. Concerning the *in-situ* strategies, solution chemical methods are mainly used to prepare MoS_2/TiO_2-based composites, where MoS_2 nanoplatelets are growing on TiO_2 basal planes [5]. As a result, 2D–2D MoS_2/TiO_2 nanosheets exhibited high activity due to the large contact area, although it was reported that heterostructures coming from solution chemical methods also show a low amount of exposed active edge sites [5].

According to some authors, TiO_2 nanosheets are preliminarily prepared by using a fluorine-based morphology controlling agent, which gives rise to the formation of Ti–F bonds on the exposed TiO_2 {001} facets [27-29]. The surface fluorine species, due to their instability during hydrothermal treatment, tend to be replaced by hydroxyl groups, which in turn absorb Mo precursors, such as MoO_4 and MoS_4 anions, which are then reduced *in-situ* by the S source to form 2D–2D MoS_2/TiO_2 nanosheets [5,8,30].

Based on these published results, in the present work, 2D–2D MoS_2/TiO_2 hierarchical nanostructures have been obtained either via *ex-situ* approach, which implies a preliminary exfoliation/fragmentation under solvent assisted ultrasonication of bulk MoS_2, followed by subsequent wet impregnation of TiO_2 nanosheets and via *in-situ* approach, from a molybdenum oxide precursor in a sulfiding atmosphere (H_2S), which gives rise to the formation of highly dispersed and strongly anchored MoS_2 particles on TiO_2 nanosheets.

The results obtained from the *ex-situ* and *in-situ* strategies will be compared in terms of morphology, structure, vibrational ad optical properties. A particular attention was paid to the different stacking degrees, to the size distribution and dispersion of the MoS_2 nanosheets, decorating the TiO_2 supports, together with the investigation of the surface sites on the main exposed faces, by

Preprints (www.preprints.org) | NOT PEER-REVIEWED | Posted: 23 November 2020 doi:10.20944/preprints202011.0579.v1

means of the adsorption of a suitable probe molecule. As a matter of fact, it is known that the CO adsorption at low temperature, as investigated by means of FT-IR spectroscopy, is a much sensitive probe to detect small differences in the Lewis acidity of the exposed sites (e.g. Ti^{4+} centers). The greater the electrophilic character of the metal cation, the greater the upshift of the signal with respect to the value of νCO in gas phase (2143 cm^{-1}) [31]. Some more, on the basis of *in-situ* strategy, it will be shown that, self-aggregation phenomena are hindered by the MoS_2/surface interaction, that is by the formation of highly dispersed and strongly anchored MoS_2 nanosheets, which in turn is favoured by sulphur doping.

2. Materials and Methods

2.1 Materials

2.1.1 Synthesis of the TiO_2 nanosheets

TiO_2 nanosheets have been obtained via a solvothermal procedure, which we briefly summarise as an extensive and detailed literature is well known on this subject [30,32]. In a typical synthesis 25 mL of $Ti(OBu)_4$ (Titanium (IV) butoxide) was poured in a 150 mL Teflon lined stainless steel reactor and 3.5 mL of concentrated hydrofluoric acid was added dropwise under stirring, at 523 K for 24 h. The resulting bluish paste was centrifuged and washed with acetone to remove the residual organics and then with water. Finally, the obtained aqueous suspension was freeze-dried obtaining a bluish powder TiO_2 nanosheets (hereafter TiO_2 n-sh). In order to remove the fluorides from the surface, TiO_2 n-sh were washed with 0.1 M NaOH, the suspension was then centrifuged (5000 rpm, 15 min), and the supernatant kept for quantification of fluorides and possibly solubilized Ti species, by ion chromatography and inductively coupled plasma mass spectrometry (ICP-MS), respectively. The paste of TiO_2 nanoparticles was recovered by centrifugation and then again centrifuged in 0.1 M HNO_3 (40 mL, 5000 rpm, 15 min) and ultrapure water, to remove the surface Na^+ ions. The effectiveness of the treatment was assessed by Auger electron spectroscopy, XPS and TOF-SIMS analyses (see the specific literature) [30,33,34]. The removal of both the bulk and the surface fluorides was achieved by calcination in air at 873 K, for 60 min, and then cooled down to 298 K in the closed furnace in approximately 10 h.

2.1.2 Synthesis of the MoS_2/TiO_2 nanosheets by *ex-situ* method

A dispersion of 2 mg of MoS_2 in 10 mL of a water/ethanol mixture (5,5 mL water and 4,5 mL ethanol) is sonicated preliminarily in an ultrasonic bath for 5 min, then subjected to further sonication at 20 kHz for 6h by means of a VCX 500 Sonics Vibracell ultrasonic processor (power 500W), equipped with a Ti alloy tapered microtip (d = 3 mm, 30% amplitude). A great intensity of cavitation can be obtained by the small diameter horn in the restricted volume of the solution, which has been placed in an ice bath to control the temperature during the whole sonication step. The obtained dark-gray and turbid solution was then centrifuged (for 30 min at 4000 rpm), thus allowing the sedimentation of bigger particles and the separation of a clear light green-yellow supernatant solution to occur [35]. The supernatant portion of the dispersed solution (about 9 mL) is then transferred to a suitable test tube, in order to study its optical properties. Subsequently, TiO_2 nanosheets powder (0,13 g) was placed on a glass disk and then on a temperature controlled heating plate (363 K), where it was impregnated with 9 mL of the sonicated MoS_2 solution. This temperature allows easy evaporation of the H_2O/EtOH solvent. Then, the obtained sample was placed in an oven at 373 K overnight. The main steps are summarised in scheme 1, left side.

2.1.3 Synthesis of the MoS_2/TiO_2 nanosheets by *in-situ* method

A clear solution of 0,066 g of ammonium heptamolybdate [AHM, $(NH_4)_6Mo_7O_{24}\times4H_2O$] in 2 mL l of distilled water under stirring at first was prepared. Then the solution was dripped onto the TiO_2

Preprints (www.preprints.org) | NOT PEER-REVIEWED | Posted: 23 November 2020 doi:10.20944/preprints202011.0579.v1

nanosheets powder (2 g) and mixed with a glass rod. The mixture was placed in an oven at 323 K overnight. With this procedure, hybrids with 3 wt.%. of Mo are obtained. The sample was then reduced in pellets by means of a hydraulic press (2,4 tons) and inserted in a gold frame (suitable for FT-IR measurements *in-situ*). Later it was placed in a muffle where the decomposition of AHM into molybdenum oxide occurred. In particular, the decomposition of AHM in MoO_x and the removal of ammonia and water, have been obtained by heat treatment in air at 673 K for 12 hours, having set a temperature ramp of 5 K per minute. At this point the sample was activated under dynamic vacuum at 673 K for 30 min, and then twice oxidized in oxygen atmosphere (40 Torr) at 673 K for 30 min. By keeping the same temperature, the oxidized sample was sulfided in the H_2S atmosphere (30 Torr) for 1 h, then outgassed. The sulfidation process was carried out twice. The main steps are summarised in scheme 1, right side.

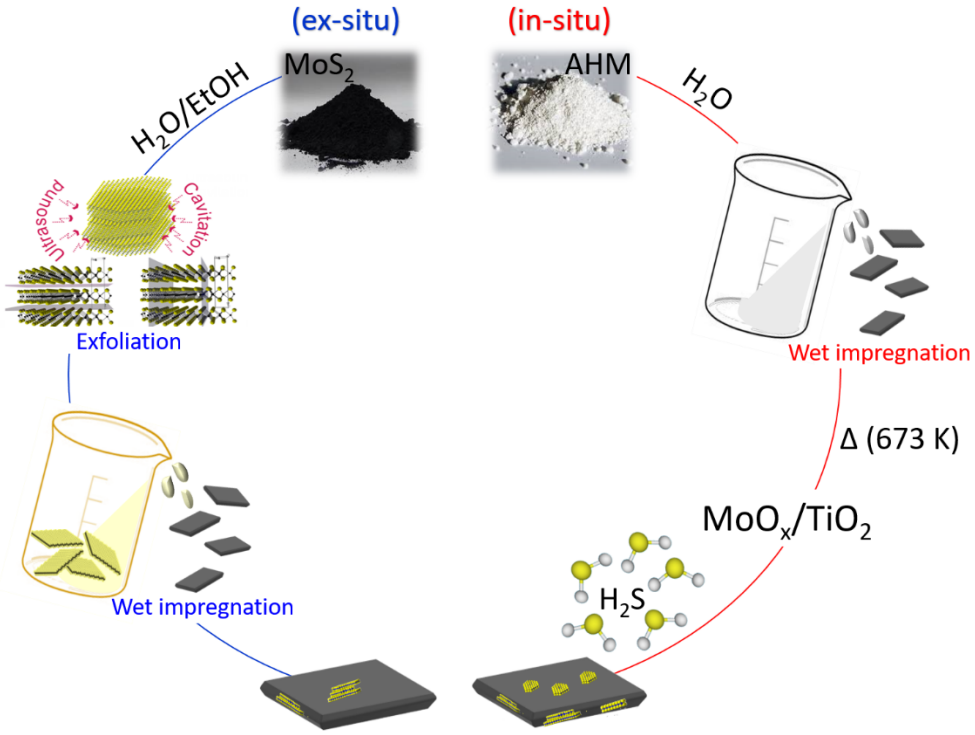

Scheme 1. Main steps of the synthesis processes of the MoS_2/TiO_2 nanosheets obtained by *ex-situ* method (on the left side) and by *in-situ* method (on the right side).

2.2 Methods

The structure and the morphology of the samples have been investigated according to the following:

(i) X-ray diffraction (XRD) patterns of samples have been collected with a PAN analytical PW3050/60 X'Pert PRO MPD diffractometer with Cu anode and Ni filter, in Bragg-Brentano configuration. The diffractograms were acquired in an interval equal to $10° \leq 2\theta \leq 80°$ with an acquisition step of 0,02°.

(ii) High-resolution transmission electron microscopy (HRTEM) images have been obtained with a JEOL 3010-UHR HRTEM microscope operating at 300 kV with a point-to-point resolution of 0,12 nm, equipped with a 2k × 2k pixels Gatan US1000 CCD camera.

(iii) Raman spectra were acquired in backscattering mode using a Renishaw In Via Raman spectrophotometer, equipped with Ar^+ laser emitting at 514.5 nm. The backscattered light was analyzed by a grid with 1200 lines/mm and detected by a CCD detector. The effects of the radiation

Preprints (www.preprints.org) | NOT PEER-REVIEWED | Posted: 23 November 2020 doi:10.20944/preprints202011.0579.v1

damage on the samples were reduced by limiting the output power to 0,5%. The vibrational properties of the samples have been investigated by means of FT-IR spectrometer Bruker IFS 66 equipped with a cryogenic MCT detector with 2 cm^{-1} resolution. To investigate the surface properties, the CO probe molecule was dosed on thin self-supported pellets by means of a gas manifold connected to the IR cell, thus allowing to perform thermal treatments under vacuum and gas dosage. The spectra have been acquired on the samples in contact with CO pressures in the 0-70 Torr range, after cooling down at the temperature of the liquid nitrogen in an IR cell designed for liquid N_2 flow conditions. The optical properties of the samples dispersed in solution have been investigated by means of transmittance mode using quartz cuvettes with an optical path of 1 cm, while the properties of the powder samples have been studied through diffuse reflectance (DR) mode. The UV-Vis-NIR spectrophotometer used is the Varian Cary UV 5000 equipped with a diffuse reflectance sphere, which acquires spectra in the 2500-190 nm wavelength range.

3. Results and Discussion

3.1 Structure and morphology by means of XRD, HRTEM and Raman analyses

3.1.1 XRD analysis

X-ray diffraction patterns of MoS_2/TiO_2 n-sh obtained by *in-situ* and *ex-situ* methods are compared together with XRD patterns of MoS_2 bulk (Fluka) and of the native TiO_2 n-sh powder (Figure 1). XRD diffraction peaks at 2θ =25.2°, 37.0°, 37.8°, 38.6°, 48.0°, 53.9° and 55.1° corresponding to (101), (103), (004), (112), (200), (105) and (211) diffraction planes of anatase (PDF card #21-1272), well match also with the native TiO_2 n-sh XRD peaks (black pattern). Together with the aforementioned XRD features, the XRD pattern after the wet impregnation with the MoS_2 diluted dispersion in H_2O/EtOH exhibits three additional weak peaks at 2θ ≅ 14.4°, 32.7° and at 39.5°, which correspond to (002), (100) and (103) diffraction planes of hexagonal MoS_2 (gray pattern). XRD diffraction fingerprints of MoS_2 are not found for the *in-situ* methods (red pattern) [36,37]. Surprisingly, although this sample has a content of 3wt.% of Mo, no XRD fingerprints of MoS_2 are present after reaction with H_2S. At this stage we can only assume that the sulphurisation products of the Mo-based species present on TiO_2 n-sh are remarkably amorphous and/or very small in size (smaller than a few nm).

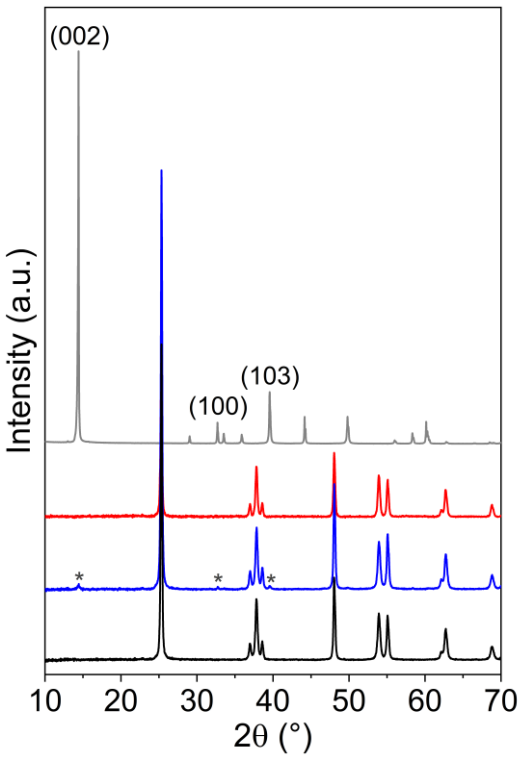

Preprints (www.preprints.org) | NOT PEER-REVIEWED | Posted: 23 November 2020 doi:10.20944/preprints202011.0579.v1

Figure 1. XRD patterns of TiO_2 anatase nano-sheet (n-sh) pre-treated at 873K (black line), of MoS_2/TiO_2 n-sh (36 mL MoS_2) prepared by *ex-situ* method (blue line), of MoS_2/TiO_2 n-sh (Mo 3 wt.%) obtained by *in-situ* approach (red line), and of pure bulk MoS_2 used as a reference material (grey line). Asterisk (*) highlight three weak diffraction features typical of MoS_2.

3.1.2 HRTEM images

The MoS_2/TiO_2 n-sh (36 mL MoS_2) sample obtained by *ex-situ* method is TEM and HRTEM imaged in Figure 2 a-d. TiO_2 nanosheets with lateral dimensions in the 50-200 nm range (Figure 2a) and thicknesses of about 30-40 nm (Figure 2b) can be observed in the lower resolution TEM images. As observed from the high-resolution TEM (HRTEM) image (Figure 2c), where nanoparticles are perpendicularly oriented to the electron beam, the TiO_2 nanosheets are highly crystalline, exposing well-defined interference fringes 3.53 Å spaced corresponding to of anatase (101) planes [38]. Cavities with rectangular shape, resulting from the nanosheet preparation, can be observed by the variation in intensity across different regions in the nanoparticles. A small nanoparticle with lateral dimension of 20 nm and 5 nm in thickness, exposes 6.5 Å spaced interference fringes that disrupted in the centre (Figure 2d). Such nanoparticle of irregular shape can be safety assigned to a MoS_2 slab with a stacking number > 5-6 [39].

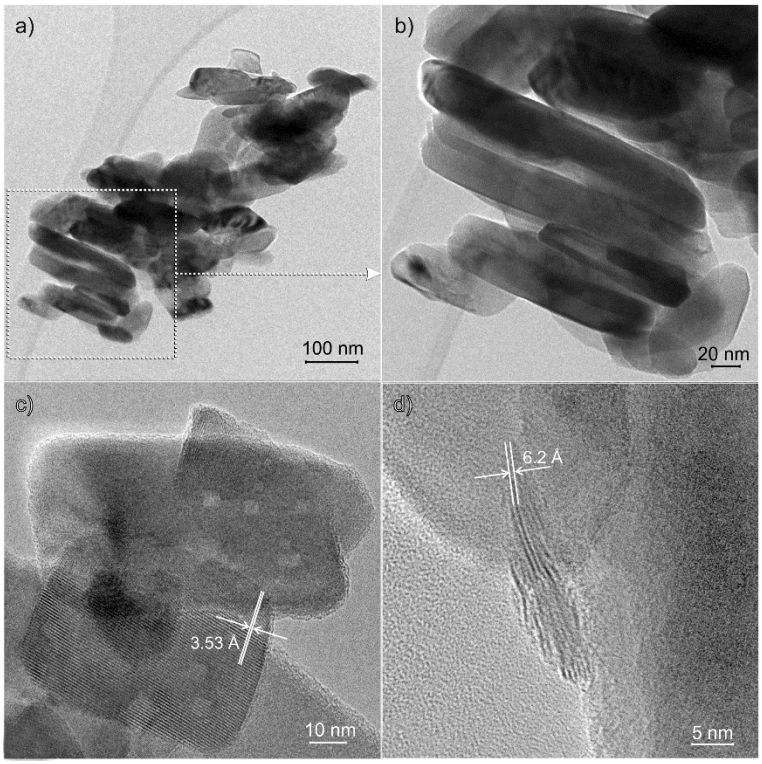

Figure 2. TEM images obtained at different magnifications of MoS_2/TiO_2 n-sh (36 mL MoS_2) prepared by *ex-situ* method.

The MoS_2/TiO_2 n-sh (Mo 3 wt.%) sample obtained by *in-situ* method is TEM and HRTEM imaged at the different magnifications in Figure 3 a-d. TiO_2 nanosheets have a prevalent orientation perpendicular to the electron beam (Figure 3a), thus exposing their basal sizes in the 30-100 nm range, although a few nanosheets expose their thicknesses of about 20-30 nm as obtained from remarkable image contrast (Figure 3b). The selected regions in Figure 3a and b are HRTEM imaged in Figure 3 c, d, where regular interference fringes 3.53 Å spaced that correspond to (101) planes of anatase are decorated with more irregular fringes. Such fringes have spacings of about 6.5-6.7 Å and can be assigned to thin MoS_2 slabs at the surface of anatase nanoparticles [36,37]. Furthermore, a stacking

Preprints (www.preprints.org) | NOT PEER-REVIEWED | Posted: 23 November 2020 doi:10.20944/preprints202011.0579.v1

number of 3 ±2 layers and basal sizes of 2-10 nm can be observed. It is worthy of attention that the MoS_2 slabs as obtained by the *in-situ* preparation appear to be thinner and more defective (i.e. basal plane interruptions, more curved structures decorating the anatase facets) with respect to the slabs obtained by the *ex-situ* preparation, despite the higher MoS_2 concentration.

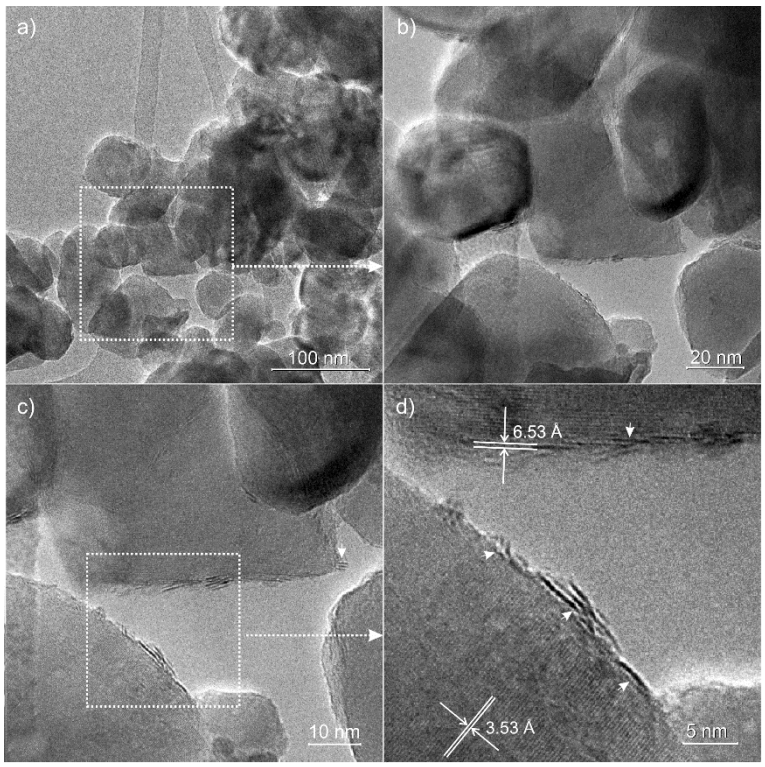

Figure 3. TEM images obtained at different magnifications of MoS_2/TiO_2 n-sh (Mo 3 wt.%) prepared by *in-situ* method.

3.1.3 Raman investigation

In Figure 4 Raman spectra, recorded with the 514 nm laser line, of MoS_2/TiO_2 n-sh obtained by *ex-situ* method (blue line) and by *in-situ* method (red line), of TiO_2 anatase nanosheet (n-sh) pretreated at 873K (black line) are compared with that of bare MoS_2, used as a reference material (grey line). Considering the Raman spectrum of pure TiO_2 nanosheets (black line), the typical anatase TiO_2 fingerprint can be recognized. As a matter of fact the four bands at 144 cm^{-1}, 396 cm^{-1}, 514 cm^{-1}, and 636 cm^{-1} are ascribed to the E_g, B_{1g}, A_{1g}, E_g Raman active modes, respectively, of the anatase phase, as described in the literature [40,41].

Moving to both the MoS_2/TiO_2 n-sh obtained by *ex-situ* method (blue line), and by *in-situ* method (red line), it can be observed that the feature centred at 396 cm^{-1}, assigned to TiO_2 anatase phase, is split into two components at 407 cm^{-1} and at 385 cm^{-1}, (blu line) and at 406 cm^{-1} and at 386 cm^{-1}, (red line) which can be ascribed to MoS_2 A_{1g} and E^1_{2g} first-order Raman active modes, respectively [20]. The A_{1g} mode corresponds to a vibration along the stacking of MoS_2, while the E^1_{2g} mode is related to the lateral extension of the MoS_2 sheets. Both signals are quite asymmetric, thus suggesting the contribution of a variety of sites located on MoS_2 boundaries characterized by slightly different nuclearity, together with a small dimensionality of the sulphide particles.

Notice that on MoS_2/TiO_2 n-sh obtained by in-situ method (Figure 4a, red line), a peak at about 227 cm^{-1} has been observed, which has been assigned to LA phonons at the **M** point [42]. According to the authors, a relationship between the intensity ratio of the LA(M) peak and each of the first-order peaks has been found, which allows a practical route to quantify defects in single-layer MoS_2 using Raman spectroscopy, thus highlighting an analogy between the LA(M) peak in MoS_2 and the D peak in graphene.

Preprints (www.preprints.org) | NOT PEER-REVIEWED | Posted: 23 November 2020 doi:10.20944/preprints202011.0579.v1

From Figure 4 a difference of the frequency values between the A_{1g} and E^1_{2g} modes of ≅ 20 cm^{-1}, for MoS_2/TiO_2 n-sh obtained by *in-situ* (red line), ≅ 22 cm^{-1} for MoS_2/TiO_2 n-sh obtained by *ex-situ* (blu line), and ≅26 cm^{-1} for the reference bare MoS_2 can be calculated. As well reported in the literature, the difference of the frequency values between A_{1g} and E^1_{2g} is indicative of the slab thickness [43]. This means that a relationship between the position of the A_{1g} and E^1_{2g} vibrational modes and the number of layers in the MoS_2 particles has been elaborated [36,44].

Moreover, most of these studies focused on materials obtained by the *ex-situ* method, via exfoliation and deposition on flat supports of bulk MoS_2. Therefore, a relationship has not been systematically investigated for MoS_2 particles grown on oxide particles as support (*in-situ* method). As matter of fact in the latter case, the shape and positions of the MoS_2 Raman bands might be directly affected by the morphology (i.e., effect of particle roughness and curvature) and surface properties of the support (i.e., preferential growth on specific crystal faces and surface defects), thus suggesting that the A_{1g} and E^1_{2g} peak positions cannot be taken as a direct reference of MoS_2 staking in the case of highly dispersed supported MoS_2. However, by applying reasonably the established relationships to our MoS_2/TiO_2 nanosheets, an average stacking of a few layers per particle could be estimated for samples coming from *in-situ* method, whereas a higher stacking level for samples obtained by *ex-situ* method can be found, in agreement with XRD and HRTEM analyses.

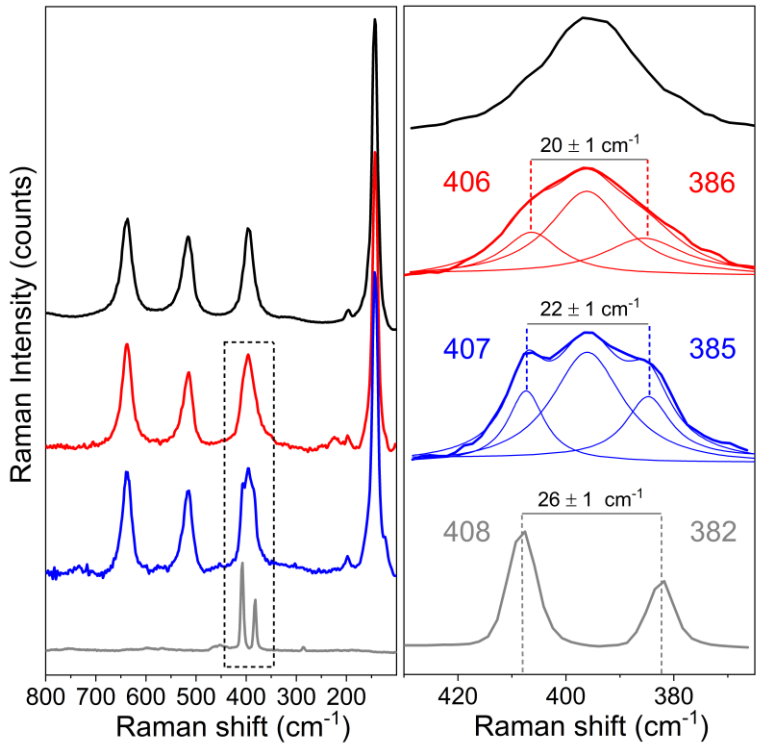

Figure 4. The panel a shows the Raman spectra, in the 800-100 cm^{-1} range, of pure bulk MoS_2 used as a reference material (grey line), of MoS_2/TiO_2 n-sh (36 mL MoS_2) obtained by *ex-situ* method (blue line), of MoS_2/TiO_2 n-sh (Mo 3 wt.%) obtained by *in-situ* method (red line), and of TiO_2 anatase nano-sheet (n-sh) pretreated at 873K (black line). All spectra were recorded with the 514 nm laser line. Enlarged views in the 425-365 cm^{-1} range reported in the panel b. The grey dashed lines in bulk MoS_2 spectrum indicate the positions of the E^1_{2g} and A_{1g} peaks, respectively. Deconvolution of the Raman patterns are shown for the MoS_2/TiO_2 n-sh (36 mL MoS_2) obtained by *ex-situ* method (blue line), and MoS_2/TiO_2 n-sh (Mo 3 wt.%) obtained by *in-situ* method (red line).

3.2 Optical properties by UV-Vis spectroscopy

Due to the close relation between optical properties of MoS_2/TiO_2 nanosheets and their morphology/structure , a characterization through diffuse reflectance spectroscopy (DRS), in the UV–Vis–NIR region, can give further structural information on the nature and properties of both the

 doi:10.20944/preprints202011.0579.v1

sulfided phase and the support, as well as on their electronic structure. In Figure 4, the UV-Vis spectra of TiO_2 anatase nanosheets, MoS_2/TiO_2 obtained by *in-situ* approach and MoS_2/TiO_2 obtained by *ex-situ* approach, are compared to that of the MoS_2 bulk, used as reference. All the spectra were recorded in the diffuse reflectance mode and converted to equivalent absorption Kubelka-Munk units. The curve of the TiO_2 nanosheets (black line) shows the typical absorption edge of TiO_2-based systems, due to the transition from O^{2-} antibonding orbital to the Ti^{4+} lowest energy orbital [19]. On the basis of the literature data [45] and other previous results [35], it comes that the spectral features of the MoS_2 reference (grey line) can be assigned as follows: (i) a first absorption threshold at about 700 nm due to a direct transition at the K point [46,47]; (ii) two sharp peaks at 680 nm and at 622 nm, on the high energy side of the 700 nm threshold, due to A and B excitonic transitions, respectively, whose separation energy can be explained with spin-orbit splitting at the top of the valence band at the K point [48]; (iii) a second threshold at about 500 nm, due to a direct transition from the deep in the valence band to the conduction band; (iv) another two excitonic transitions at 482 nm (C), and at 399 nm (D), also associated with the 500 nm threshold transition [45]; (v) and a third threshold at about 350 nm due to transitions from deep in the valence band [46]. The curve of the MoS_2/TiO_2 hybrid system obtained by *in-situ* approach (red line) shows a continuum and wide absorption over the UV-visible range, due to the presence above the valence band, of new electronic states coming from the sulphur-oxygen exchange at the surface of TiO_2 nanosheets. These states are related to the mixing of S 3p atomic orbitals with the valence band of TiO_2 [19]. The contribution of reduced molybdenum species on TiO_2 defective nanosheets can be also considered, although hidden inside the wide and intense absorption, being a further proof of the formation of thin MoS_2 platelets [35,43]. The typical bands relative to the MoS_2 excitonic bands A and B are shifted to higher energies than the MoS_2 bulk, suggesting a quantum confinement of the excitons, due to the low dimensionality of the MoS_2 particles, which is in agreement with the HRTEM and XRD results. The features in the 400-500 nm range, already explained with the C and D excitons of MoS_2, are overlapping inside a broad band, as expected for a highly dispersed supported material.

Similar features are present in the MoS_2/TiO_2 hybrid obtained through the ex-situ approach (blue line), although slightly downward shifted, as compared to the in-situ sample. Considering more in detail both the systems, obtained by in-situ and ex-situ approaches (red and blue lines, respectively), if compared to those of the reference MoS_2 bulk, it can be observed that the energy values of A and B excitons are only slightly upward shifted, whereas significant shifts are observed for C and D excitons envelope, according to the fact that quantum size effects are affecting C and D bands in a more remarkable way [46].

Notice that quantum size effects have been discussed in terms of low dimensionality of the MoS_2 particles along the c direction, being the particles characterized by a low number of layers, but the small size of the MoS_2 platelets along the ''in-plane'' a and b directions can have also a role [48]. According to this, we can conclude that the sample synthesized via the *in-situ* approach has smaller MoS_2 particles than the sample synthesized via the *ex-situ* method, being some level of particle stacking observed in the last case (as HRTEM imaged in Figure 2 and Figure 3).

Preprints (www.preprints.org) | NOT PEER-REVIEWED | Posted: 23 November 2020 doi:10.20944/preprints202011.0579.v1

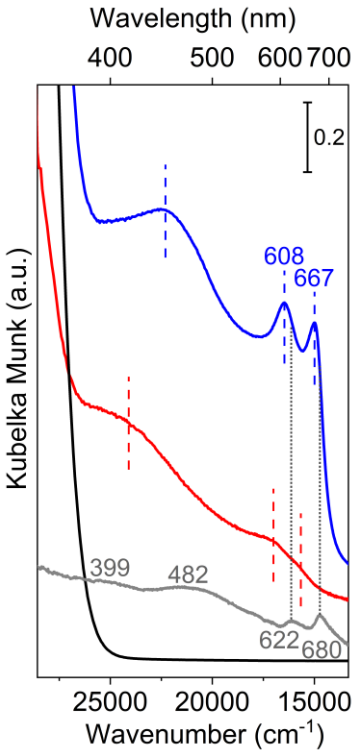

Figure 4. UV-Vis spectra of TiO_2 anatase nano-sheet (n-sh) pretreated at 873K (black line), of pure bulk MoS_2 used as a reference material (grey line), of MoS_2/TiO_2 n-sh (Mo 3 wt.%) obtained by *in-situ* approach (red line), and of MoS_2/TiO_2 n-sh (36 mL MoS_2) prepared by *ex-situ* method (blue line). The grey dotted lines indicate the positions of the typical MoS_2 A and B excitonic transitions. The blue and red dashed lines of MoS_2/TiO_2 samples show the shift with respect to the bulk MoS_2. All spectra were recorded in the diffuse reflectance mode and converted to equivalent absorption Kubelka–Munk units.

3.3 Surface vibrational properties by FT-IR

FTIR spectra of CO adsorbed at liquid nitrogen temperature, at decreasing coverages up to the residual pressure of $4 \cdot 10^{-4}$ Torr, on the surface of TiO_2 n-sh (pretreated at 873 K), of MoS_2/TiO_2 n-sh (36 mL MoS_2) (pretreated at 673K) and of MoS_2/TiO_2 n-sh (Mo 3 wt.%) (pretreated at 673 K) are shown in Figure 5. The main feature of the CO adsorbed on the TiO_2 n-sh sample at 77K (Figure 5, on the top) is the band at 2159 cm^{-1} assigned to the CO molecules adsorbed on Ti^{4+} sites on (1x4) reconstructed (001) surfaces, together with a minor feature observed at 2179 cm^{-1} , that has been assigned to CO molecules adsorbed on (101) surfaces, less extensive than (001), according to the data and models reported in the literature [30]. Some more a weak shoulder at ca. 2155 cm^{-1}, which is hidden within the envelope of the band on the low frequency side, due to CO species interacting with the residual surface OH groups, can be detected. Notice that the band at 2159 cm^{-1} is fully reversible upon CO outgassing, whereas the peak at ~2179 cm^{-1} remains almost unaffected at the temperature of the experiment. Furthermore, the maximum of the 2159 cm^{-1} band undergoes a quite negligible upward frequency shift upon decreasing CO pressure, approaching the singleton ν(CO), plausibly due to the fading away of weak dynamic and static interactions within CO adlayer. The low upshift of the singleton mode with respect to the CO stretching mode in gas phase (2143 cm^{-1}), together with the complete reversibility upon CO outgassing are explained with the low electrophilicity/reduced acidity of the Ti^{4+} sites on (001) surfaces, because of a screened electrostatic potential at these Ti sites, which are strongly bound to two oxygens. This agrees with the weakness of their interaction with CO [19].

Surprisingly, moving to the spectra of CO adsorbed on the surface of MoS_2/TiO_2 nanosheets obtained by *ex-situ* approach (Figure 5, on the bottom left side), no vibrational modes associated with

 doi:10.20944/preprints202011.0579.v1

molybdenum species are observed, being the absorption bands mainly due to CO interaction with the support, which can be explained with the very low concentration of Mo^{x+} species. However, a general decrease in intensity of the main features with respect to pure TiO_2 n-sh can be highlighted, confirming the involvement of a few Mo species in the formation of rare MoS_2 slabs, which cover small regions on TiO_2 nanosheets, thus making the (001) and (101) faces still available toward CO adsorption. Conversely from the CO spectra on MoS_2/TiO_2 nanosheets (Mo 3 wt.%) obtained by *in-situ* approach (Figure 5, on the bottom right side) significant changes can be observed. At higher frequencies, the features at 2179 cm^{-1} and 2159 cm^{-1}, already assigned on previous systems to the CO molecules adsorbed on Ti^{4+} sites on (101) and (001) surfaces, respectively, are also observed, but with a different intensity ratio. Considering the asymmetry on the low frequency side of the band centered at 2159 cm^{-1}, modes due to physically adsorbed CO on heterogeneous surface sites, including residual OH groups and/or sulphur anions on basal planes of crystalline MoS_2 cannot be ruled out [49]. However, in the 2130 cm^{-1}-2050 cm^{-1} range two significant bands, at 2117 cm^{-1} and 2066 cm^{-1}, are observed which are absent on the MoS_2/TiO_2 n-sh sample obtained by *ex-situ* method (Figure 5 on bottom, left side). The appearance of these features, downshifted with respect to CO free molecule (2143 cm^{-1}), indicates the formation of surface sites characterized by π-backdonation character [50]. They have been already assigned in the past [51] to carbonyl species formed on a large variety of coordinatively unsaturated Mo^{x+} centres ($x < 4$) on highly defective situations (Mo–S) [43,52]. In particular, the band at 2117 cm^{-1} can be ascribed to the Mo^{x+} species ($x < 4$) located on defective sites (e.g. edges), while the 2066 cm^{-1} one could be due to the interaction of CO with Mo^{x+} species ($x < 4$) located on highly exposed sites such as corners [36]. Such bands are the last ones to disappear by outgassing and this is a further confirmation of the presence of isolated and coordinatively unsaturated molybdenum species on defective sites associated with the formation of sulphur vacancies [40].

Preprints (www.preprints.org) | NOT PEER-REVIEWED | Posted: 23 November 2020 doi:10.20944/preprints202011.0579.v1

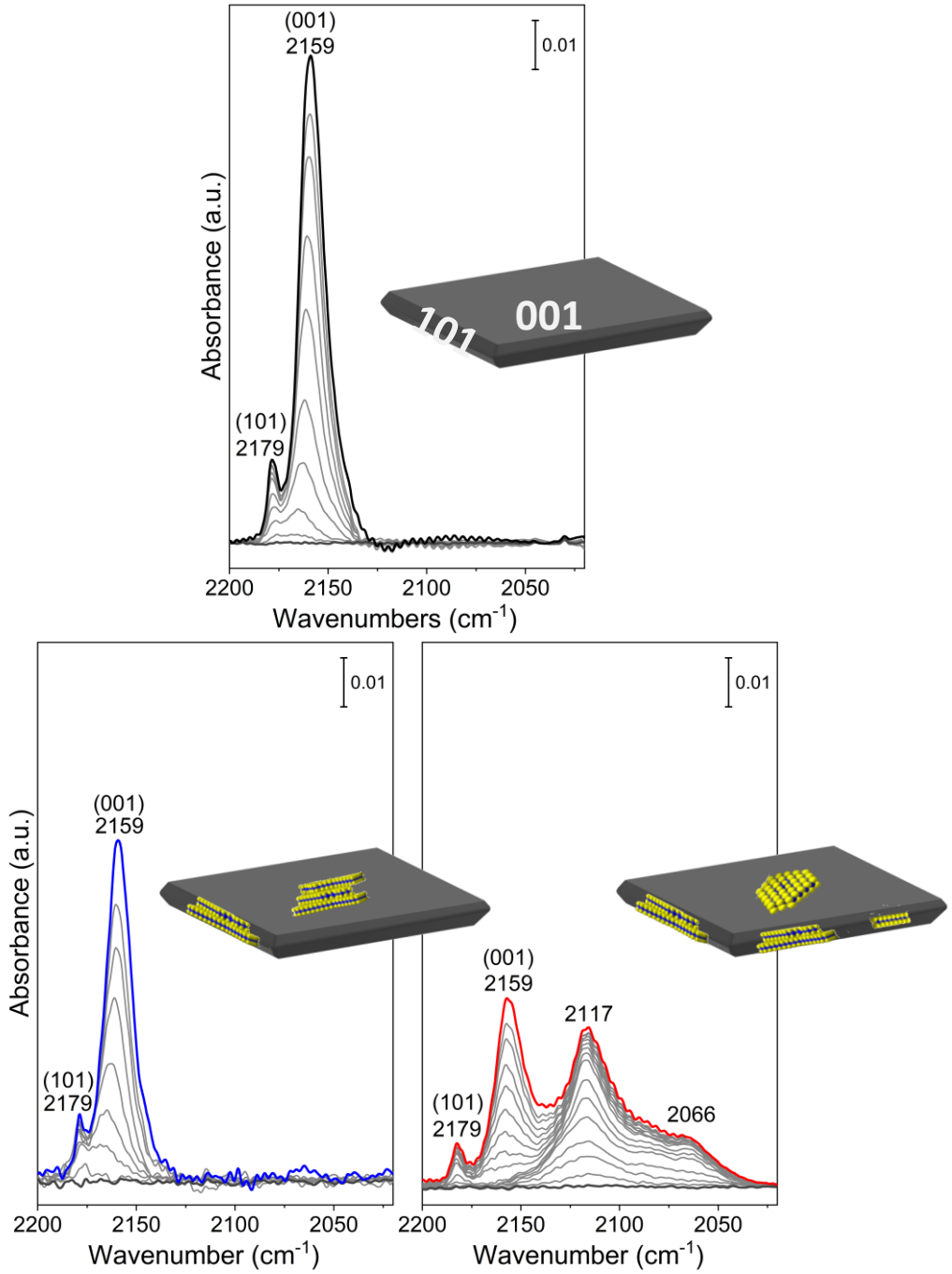

Figure 5 FT-IR spectra, recorded at 77K, of CO (30 Torr) adsorbed at decreasing coverage on the surface of: TiO_2 anatase nano-sheet (n-sh) pretreated at 873K (on the top), MoS_2/TiO_2 n-sh (36 mL MoS_2) obtained by *ex-situ* method (on the bottom, left side), MoS_2/TiO_2 n-sh (Mo 3 wt.%) obtained by *in-situ* method (on the bottom, right side).

FTIR spectra of CO adsorbed (at 77 K at maximum coverage) on TiO_2 n-sh, MoS_2/TiO_2 n-sh (via *ex-situ* method) and MoS_2/TiO_2 n-sh (via *in-situ* method) are compared in Figure 6 (black, blue and red curves, respectively) aiming to investigate the effects of the different synthesis method on the surface properties of the two systems MoS_2/TiO_2 n-sh, as compared to the pure TiO_2-nsh sample. From a first analysis, it comes out that i) the spectra of both the MoS_2/TiO_2 n-sh samples are characterized by a lower intensity of the typical signals at 2179 cm^{-1} and 2159 cm^{-1} due to the adsorption of CO on the (101) and (001) surfaces, respectively; and ii) only for the MoS_2/TiO_2 n-sh sample prepared via *in-situ* method the signals in the range 2130 cm^{-1}-2050 cm^{-1}, associated with the Mo^{x+} species in reduced states (x <4), are observed. The general decrease in intensity can be associated

Preprints (www.preprints.org) | NOT PEER-REVIEWED | Posted: 23 November 2020 doi:10.20944/preprints202011.0579.v1

with the presence of new Mo^{x+} species masking the Ti^{4+} sites, which are no longer available for interactions with CO. Such phenomenon is more evident for the MoS_2/TiO_2 n-sh prepared via *in-situ* approach due to the higher MoS_2 concentration with respect to the sample obtained via *ex-situ* method. Furthermore, the absence of the components assigned to Mo^{x+} species in reduced states (x <4) for the sample obtained by *ex-situ* method can be explained by the fact that the Mo^{x+} species are present only on defective sites belonging to thin and uniformly distributed MoS_2 slabs. Indeed, the HRTEM images (Figure 3) have shown thinner and more defective MoS_2 slabs for the sample prepared by *in-situ* approach. Conversely, the preparation via *ex-situ* approach gives rise to a heterogeneous and minor amount of MoS_2 slabs anchored to the surface of TiO_2 nanosheets, which are characterized by a higher level of stacking and therefore became less reactive.

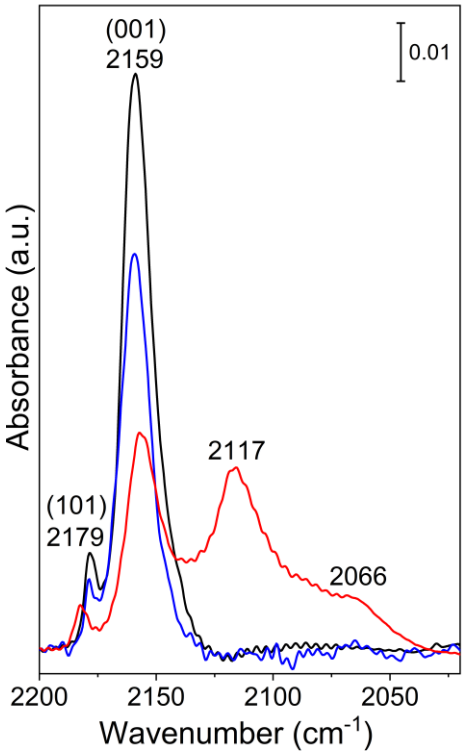

Figure 6. FT-IR spectra, recorded at 77K, at the maximum coverage of CO (30 Torr) adsorbed on the surface of TiO_2 anatase nano-sheet (n-sh) pretreated at 873K (black curve), of MoS_2/TiO_2 n-sh (36 mL MoS_2) obtained by *ex-situ* method (blue curve), and of MoS_2/TiO_2 n-sh (Mo 3 wt.%) obtained by *in-situ* approach (red curve).

4. Conclusions

MoS_2/TiO_2 heterostructures, consisting of MoS_2 slabs with different stacking order covering TiO_2 nanosheets have been synthesized following *ex-situ* and *in-situ* method. Combining XRD, HRTEM , Raman, UV-visible and FTIR data, the characteristics of MoS_2/TiO_2 heterostructures obtained from *ex-situ* and *in-situ* preparations were compared, highlighting the role played by the synthesis processes in affecting morphology, structure, stacking order and defectivity. More in detail, MoS_2 slabs as obtained by the *in-situ* preparation appear to be thinner and more defective (i.e. basal plane interruptions, more curved structures decorating the anatase facets) with respect to the slabs obtained by the *ex-situ* preparation, despite the higher MoS_2 concentration.

In particular, a stacking number of 3 ±2 layers and basal sizes of 2-10 nm for MoS_2 particles on MoS_2/TiO_2 nanosheets coming from *in-situ* method could be estimated, whereas a stacking number > 5-6 and lateral dimension of 20 nm for MoS_2 particles on MoS_2/TiO_2 nanosheets obtained by *ex-situ* method can be found. Some more from the HRTEM analysis of samples obtained by *in-situ* method, the presence of more curved MoS_2 slabs decorating the profile of the anatase nanosheets means that a significant grafting of MoS_2 particles at the (001) and (101) anatase facelets is occurring. Therefore,

we can conclude that the sulfidation process has a role in affecting the reactivity of the support matrix as well, which in turn affects the MoS_2/support interaction. The low dimensionality of the MoS_2 particles on MoS_2/TiO_2 nanosheets synthesized via the *in-situ* approach with respect to those obtained by the *ex-situ* method, already explained in terms of quantum size effects, has been further confirmed from the UV-Vis results.

Lastly, from FTIR spectra, the presence of new Mo^{x+} species on defective sites, masking the Ti^{4+} sites, which are no longer available for interactions with CO, is a further confirmation that MoS_2 slabs are thinner, more defective and uniformly distributed for the sample prepared by *in-situ* approach, whereas MoS_2 slabs obtained via *ex-situ* approach are more heterogeneously dispersed with a higher level of stacking and therefore low reactivity.

It is so concluded that the morphology and dispersion of hybrid composites can be tailored by fine-tuning the preparation and activation conditions, also plausibly addressing the interface structure and then the charge control.

Author Contributions: D.S., F.C., T.V., and R.S. wrote and organized the manuscript. T.V. and R.S. performed experiments and characterizations. F.P. and G.M. provided a substantial contribution to the work, in particular, F.P. contributed to sample preparation. All authors approved it for publication.

Funding: This work was supported by MIUR (Ministero dell'Istruzione, dell'Università e della Ricerca), INSTM Consorzio and NIS (Nanostructured Interfaces and Surfaces) Inter-Departmental Center of University of Torino.

Acknowledgments: The authors thank the Laboratory of the Chemistry Department and, in particular, Dr. M. Signorile, Dr. A. Damin, Prof. F. Bonino, Prof. V. Maurino, Dr. S. Cravanzola and Dr. M. C. Valsania.

Conflicts of Interest: The authors declare no conflict of interest.

References

1. Chatterjee, D.; Mahata, A. Visible light induced photodegradation of organic pollutants on dye adsorbed TiO_2 surface. *J. Photochem. Photob. A Chem.* **2002**, *153*, 199—204.
2. Matos, J.; García, A.; Zhao, L.; Titirici, M.M. Solvothermal Carbon-Doped TiO_2 Photocatalyst for the Enhanced Methylene Blue Degradation Under Visible Light. *Appl. Catal. A Gen.* **2010**, *390*, 175—182.
3. Cheng, Y.; Geng, H.; Huang, X. Advanced water splitting electrocatalysts via the design of multicomponent heterostructures. *Dalt. Trans.* **2020**, *49*, 2761—2765.
4. Uddin, M.J.; Daramola, D.E.; Velasquez, E.; Dickens, T.J.; Yan, J.; Hammel, E. A high efficiency 3D photovoltaic microwire with carbon nanotubes (CNT)-quantum dot (QD) hybrid interface. *Phys. Status Solidi RRL* **2014**, *8*, 898—903.
5. Chen, B.; Meng, Y.; Sha, J.; Zhong, C.; Hu, W.; Zhao, N. Preparation of MoS_2/TiO_2 based nanocomposites for photocatalysis and rechargeable batteries: Progress, challenges, and perspective. *Nanoscale* **2018**, *10*, 34—68.
6. Wang, H.; Liu, F.; Fu, W.; Fang, Z.; Zhou, W.; Liu, Z. Two-dimensional heterostructures: Fabrication, characterization, and application. *Nanoscale* **2014**, *6*, 12250—12272.
7. Wang, Z.; Mi, B. Environmental Applications of 2D Molybdenum Disulfide (MoS_2) Nanosheets. *Env. Sci. Technol.* **2017**, *51*, 8229—8244.
8. Yuan, Y.J.; Ye, Z.J.; Lu, H.W.; Hu, B.; Li, Y.H.; Chen, D.Q.; Zhong, J.S.; Yu, Z.T.; Zou, Z.G. Constructing Anatase TiO_2 Nanosheets with Exposed (001) Facets/Layered MoS_2 Two-Dimensional Nanojunctions for Enhanced Solar Hydrogen Generation. *ACS Catal.* **2016**, *6*, 532—541.
9. Goswami, N.; Giri, A.; Pal, S.K. MoS_2 nanocrystals confined in a dna matrix exhibiting energy transfer. *Langmuir* **2013**, *29*, 11471—11478.

10. Lee, Y.H.; Zhang, X.Q.; Zhang, W.; Chang, M.T.; Lin, C.T.; Chang, K.D.; Yu, Y.C.; Wang, J.T.W.; Chang, C.S.; Li, L.J., et al. Synthesis of large-area MoS_2 atomic layers with chemical vapor deposition. *Adv. Mater.* **2012**, *24*, 2320−2325.
11. Stephenson, T.; Li, Z.; Olsen, B.; Mitlin, D. Lithium ion battery applications of molybdenum disulfide (MoS_2) nanocomposites. *En. Environ. Sci.* **2014**, *7*, 209−231.
12. Lin, Y.; Ren, P.; Wei, C. Fabrication of MoS_2/TiO_2 heterostructures with enhanced photocatalytic activity. *CrystEngComm* **2019**, *21*, 3439−3450.
13. Wan, J.; Lacey, S.D.; Dai, J.; Bao, W.; Fuhrer, M.S.; Hu, L. Tuning two-dimensional nanomaterials by intercalation: Materials, properties and applications. *Chem. Soc. Rev.* **2016**, *45*, 6742−6765.
14. Sreepal, V.; Yagmurcukardes, M.; Vasu, K.S.; Kelly, D.J.; Taylor, S.F.R.; Kravets, V.G.; Kudrynskyi, Z.; Kovalyuk, Z.D.; Patanè, A.; Grigorenko, A.N., et al. Two-Dimensional Covalent Crystals by Chemical Conversion of Thin van der Waals Materials. *Nano Lett.* **2019**, *19*, 6475−6481.
15. Zhao, X.; Song, P.; Wang, C.; Riis-Jensen, A.C.; Fu, W.; Deng, Y.; Wan, D.; Kang, L.; Ning, S.; Dan, J., et al. Engineering covalently bonded 2D layered materials by self-intercalation. *Nature* **2020**, *581*, 171−177.
16. Geim, A.K.; Grigorieva, I.V. Van der Waals heterostructures. *Nature* **2013**, *499*, 419−425.
17. Pumera, M.; Loo, A.H. Layered transition-metal dichalcogenides (MoS_2 and WS_2) for sensing and biosensing. *TrAC* **2014**, *61*, 49−53.
18. Guo, L.; Yang, Z.; Marcus, K.; Li, Z.; Luo, B.; Zhou, L.; Wang, X.; Du, Y.; Yang, Y. MoS_2/TiO_2 heterostructures as nonmetal plasmonic photocatalysts for highly efficient hydrogen evolution. *En. Environm. Sci.* **2018**, *11*, 106−114.
19. Scarano, D.; Cesano, F.; Zecchina, A. MoS_2 Domains on TiO_2 -Based Nanostructures: Role of Titanate/TiO_2 Transformation and Sulfur Doping on the Interaction with the Support. *J. Phys. Chem. C* **2019**, *123*, 7799−7809.
20. Cravanzola, S.; Sarro, M.; Cesano, F.; Calza, P.; Scarano, D. Few-layer MoS_2 nanodomains decorating TiO_2 nanoparticles: A case study for the photodegradation of carbamazepine. *Nanomaterials* **2018**, *8*, 207.
21. Kumar, S.G.; Devi, L.G. Review on Modified TiO_2 Photocatalysis under UV/Visible Light: Selected Results and Related Mechanisms on Interfacial Charge Carrier Transfer Dynamics. *J. Phys. Chem. A* **2011**, *115*, 13211−13241.
22. Rao, C.N.R.; Maitra, U.; Waghmare, U.V. Extraordinary attributes of 2-dimensional MoS_2 nanosheets. *Chem. Phys. Lett.* **2014**, *609*, 172−183.
23. Zhou, X.; Dong, H. A Theoretical Perspective on Charge Separation and Transfer in Metal Oxide Photocatalysts for Water Splitting. *ChemCatChem* **2019**, *11*, 3688−3715.
24. Selçuk, S.; Selloni, A. Surface Structure and Reactivity of Anatase TiO_2 Crystals with Dominant {001} Facets. *J. Phys. Chem. C* **2013**, *117*, 6358−6362.
25. Yang, X.; Huang, H.; Jin, B.; Luo, J.; Zhou, X. Facile synthesis of MoS_2/B-TiO_2 nanosheets with exposed {001} facets and enhanced visible-light-driven photocatalytic H_2 production activity. *RSC Adv.* **2016**, *6*, 107075−107080.
26. Chen, H.; Wen, X.; Zhang, J.; Wu, T.; Gong, Y.; Zhang, X.; Yuan, J.; Yi, C.; Lou, J.; Ajayan, P.M., et al. Ultrafast formation of interlayer hot excitons in atomically thin MoS_2/WS_2 heterostructures. *Nature Commun.* **2016**, *7*, 12512.
27. Dozzi, M.V.; Selli, E. Specific Facets-Dominated Anatase TiO_2: Fluorine-Mediated Synthesis and Photoactivity. *Catalysts* **2013**, *3*, 455−485.

28. Gordon, T.R.; Cargnello, M.; Paik, T.; Mangolini, F.; Weber, R.T.; Fornasiero, P.; Murray, C.B. Nonaqueous Synthesis of TiO_2 Nanocrystals Using TiF4 to Engineer Morphology, Oxygen Vacancy Concentration, and Photocatalytic Activity. *JACS* **2012**, *134*, 6751−6761.
29. Uddin, M.J.; Cesano, F.; Chowdhury, A.R.; Trad, T.; Cravanzola, S.; Martra, G.; Mino, L.; Zecchina, A.; Scarano, D. Surface Structure and Phase Composition of TiO_2 P25 Particles After Thermal Treatments and HF Etching. *Frontiers in Materials* **2020**, *7*, 192.
30. Mino, L.; Pellegrino, F.; Rades, S.; Radnik, J.; Hodoroaba, V.-D.; Spoto, G.; Maurino, V.; Martra, G. Beyond Shape Engineering of TiO_2 Nanoparticles: Post-Synthesis Treatment Dependence of Surface Hydration, Hydroxylation, Lewis Acidity and Photocatalytic Activity of TiO_2 Anatase Nanoparticles with Dominant {001} or {101} Facets. *ACS Appl. Nano Mater.* **2018**, *1*, 5355−5365.
31. Davydov, A. *Theoretical Fundamentals and Experimental Considerations of the Spectroscopic Methods Used in Surface Chemistry*; Wiley: 2003; 10.1002/0470867981.ch1pp. 1−25.
32. Pellegrino, F.; Sordello, F.; Mino, L.; Minero, C.; Hodoroaba, V.-D.; Martra, G.; Maurino, V. Formic Acid Photoreforming for Hydrogen Production on Shape-Controlled Anatase TiO_2 Nanoparticles: Assessment of the Role of Fluorides, {101}/{001} Surfaces Ratio, and Platinization. *ACS Catal.* **2019**, *9*, 6692−6697.
33. Han, X.; Kuang, Q.; Jin, M.; Xie, Z.; Zheng, L. Synthesis of titania nanosheets with a high percentage of exposed (001) facets and related photocatalytic properties. *JACS* **2009**, *131*, 3152−3153.
34. Zhang, Y.; Cai, J.; Ma, Y.; Qi, L. Mesocrystalline TiO_2 nanosheet arrays with exposed {001} facets: Synthesis via topotactic transformation and applications in dye-sensitized solar cells. *Nano Res.* **2017**, *10*, 2610−2625.
35. Muscuso, L.; Cravanzola, S.; Cesano, F.; Scarano, D.; Zecchina, A. Optical, vibrational, and structural properties of MoS_2 nanoparticles obtained by exfoliation and fragmentation via ultrasound cavitation in isopropyl alcohol. *J. Phys. Chem. C* **2015**, *119*, 3791−3801.
36. Cesano, F.; Bertarione, S.; Piovano, A.; Agostini, G.; Rahman, M.M.; Groppo, E.; Bonino, F.; Scarano, D.; Lamberti, C.; Bordiga, S., et al. Model oxide supported MoS_2 HDS catalysts: Structure and surface properties. *Catal. Sci. Technol.* **2011**, *1*, 123−136.
37. Cravanzola, S.; Cesano, F.; Magnacca, G.; Zecchina, A.; Scarano, D. Designing rGO/MoS_2 hybrid nanostructures for photocatalytic applications. *RSC Advances* **2016**, *6*, 59001−59008.
38. Cesano, F.; Agostini, G.; Scarano, D. Nanocrystalline TiO_2 micropillar arrays grafted on conductive glass supports: microscopic and spectroscopic studies. *Thin Solid Films* **2015**, *590* 200−206.
39. Sharma, A.; Mahlouji, R.; Wu, L.; Verheijen, M.A.; Vandalon, V.; Balasubramanyam, S.; Hofmann, J.P.; Erwin Kessels, W.M.M.; Bol, A.A. Large area, patterned growth of 2D MoS_2 and lateral MoS_2–WS_2 heterostructures for nano- and opto-electronic applications. *Nanotechnol.* **2020**, *31*, 255603.
40. Cravanzola, S.; Cesano, F.; Gaziano, F.; Scarano, D. Sulfur-doped TiO_2: Structure and surface properties. *Catalysts* **2017**, *7*, 214.
41. Kumar, S.; Shakya, J.; Mohanty, T. Probing interfacial charge transfer dynamics in MoS_2/TiO_2 nanocomposites using scanning Kelvin probe for improved photocatalytic response. *Surf. Sci.* **2020**, *693*, 121530.
42. Mignuzzi, S.; Pollard, A.J.; Bonini, N.; Brennan, B.; Gilmore, I.S.; Pimenta, M.A.; Richards, D.; Roy, D. Effect of disorder on Raman scattering of single-layer MoS_2. *Phys. Rev. B* **2015**, *91*, 195411.
43. Cravanzola, S.; Cesano, F.; Gaziano, F.; Scarano, D. Carbon domains on MoS_2/TiO_2 system via catalytic acetylene oligomerization: Synthesis, structure, and surface properties. *Front. Chem.* **2017**, *5*, 91.

44. Lee, C.; Yan, H.; Brus, L.E.; Heinz, T.F.; Hone, J.; Ryu, S. Anomalous lattice vibrations of single- and few-layer MoS_2. *ACS Nano* **2010**, *4*, 2695−2700.
45. Wilcoxon, J.P.; Newcomer, P.P.; Samara, G.A. Synthesis and optical properties of MoS_2 and isomorphous nanoclusters in the quantum confinement regime. *J. Appl. Phys.* **1997**, *81*, 7934.
46. Cravanzola, S.; Muscuso, L.; Cesano, F.; Agostini, G.; Damin, A.; Scarano, D.; Zecchina, A. MoS_2 nanoparticles decorating titanate-nanotube surfaces: Combined microscopy, spectroscopy, and catalytic studies. *Langmuir* **2015**, *31*, 5469−5478.
47. Ramakrishna Matte, H.S.S.; Gomathi, A.; Manna, A.K.; Late, D.J.; Datta, R.; Pati, S.K.; Rao, C.N.R. MoS_2 and WS_2 Analogues of Graphene. *Angew. Chem. Int. Ed.* **2010**, *49*, 4059−4062.
48. Shi, H.; Yan, R.; Bertolazzi, S.; Brivio, J.; Gao, B.; Kis, A.; Jena, D.; Xing, H.G.; Huang, L. Exciton dynamics in suspended monolayer and few-layer MoS_2 2D crystals. *ACS Nano* **2013**, *7*, 1072−1080.
49. Tsyganenko, A.A.; Can, F.; Travert, A.; Maugé, F. FTIR study of unsupported molybdenum sulfide—in situ synthesis and surface properties characterization. *Appl. Catal. A Gen.* **2004**, *268*, 189−197.
50. Bolis, V.; Barbaglia, A.; Bordiga, S.; Lamberti, C.; Zecchina, A. Heterogeneous Nonclassical Carbonyls Stabilized in Cu(I)− and Ag(I)−ZSM-5 Zeolites: Thermodynamic and Spectroscopic Features. *J. Phys. Chem B* **2004**, *108*, 9970−9983.
51. Bachelier, J.; Duchet, J.C.; Cornet, D. On the promoting effect in sulfided Ni⊙Mo/Al_2O_3 catalysts as studied by chemisorption. *J. Catal.* **1984**, *87*, 283−291.
52. Maugé, F.; Lamotte, J.; Nesterenko, N.S.; Manoilova, O.; Tsyganenko, A.A. FT-IR study of surface properties of unsupported MoS_2. *Catal. Today* **2001**, *70*, 271−284.